

HF-Free Synthesis of α -Zirconium Phosphate and Its Use as Ion Exchanger for Separation of Nd(III) and Dy(III) from a Ternary Co–Nd–Dy System

Junhua Xu¹ · Elmo Wiikinkoski¹ · Risto Koivula¹ · Wenzhong Zhang¹ · Burcak Ebin² · Risto Harjula¹

Published online: 10 April 2017
© The Minerals, Metals & Materials Society 2017

Abstract The recovery of Nd and Dy from a ternary Co–Nd–Dy system using layered crystalline zirconium phosphate (α -ZrP) was investigated. α -ZrP was synthesized by the refluxing method, and subsequently characterized by sodium hydroxide titration, Fourier transform-infrared spectrometry, thermogravimetry, scanning electron microscopy, and X-ray diffraction. The selectivity and ion exchange kinetics of the α -ZrP material were determined with regard to the individual elements. The influence of solution pH on the uptake was studied in ternary 1 and 2 mM equimolar solutions. The results showed that in acidic solution (pH 1–3), very little Co was taken up, while Nd and Dy uptakes were at reasonable levels (0.5–0.6 meq/g). The uptake isotherms of Nd, Dy, and Co were measured separately at pH 2.5 and 4.5 in ternary equimolar solution series. At pH 4.5, the loading capacities were about 0.2 meq/g for Co, 1.1 meq/g for Nd, and 1.5 meq/g for Dy. Dy was thus clearly preferred over Nd by α -ZrP. The loading of an α -ZrP column showed a similar preferred pattern. Nitric acid eluent removed Co, Nd, and Dy, but there was no separation of the metals in the eluate. A mixture of nitric and phosphoric acids, however, produced a strong separation. Co was very weakly retained in the column, and the ratio Dy/Nd in the eluent was in the range

of 2–7. Thus, the α -ZrP material showed encouraging ion exchange properties for the separation and recycling of Nd and Dy from a ternary Co–Nd–Dy system. Much more work is needed, however, to develop a practical separation flowsheet.

Keywords Zirconium phosphate · NdFeB magnet · Green synthesis · Ion exchange · REE separation

Introduction

In recent years, rare earth elements (REEs) have been increasingly needed for the development of the worldwide green economy of permanent magnets, nickel metal hydride batteries, lamp phosphors, catalysts, and so on [1]. In 2010, the European Commission considered REEs as a critical raw materials group with the highest supply risk. Neodymium (Nd), europium (Eu), terbium (Tb), dysprosium (Dy), and yttrium (Y) were listed as the five most critical REEs by the U.S. Department of Energy in 2011. In addition, it is estimated that over the subsequent 25 years, the demand for Nd and Dy will rise by 700 and 2600%, respectively [2]. Nd is the most common REE in NdFeB magnets. Dy is often added to NdFeB magnets to increase their temperature stability against demagnetization. NdFeB magnets with added Dy have wide application in electric and hybrid electric vehicle motors, wind turbine generators, computers, peripherals, etc. It was estimated that in 2007, 66% of all NdFeB magnets used could be attributed to computer, wind turbine, and automotive applications. Of these magnets, 80% contained Dy in addition to Nd. At present, recycling of NdFeB magnets is of potential technical feasibility, if efficient physical dismantling and separation techniques, and metallurgical separation and

The contributing editor for this article was T. Hirato.

✉ Junhua Xu
junhua.xu@helsinki.fi

¹ Laboratory of Radiochemistry, Department of Chemistry, University of Helsinki, 00560 Helsinki, Finland

² Nuclear Chemistry and Industrial Materials Recycling, Department of Chemistry and Chemical Engineering, Chalmers University of Technology, 412 96 Gothenburg, Sweden

refining methods are available in the future [3]. In fact, due to inefficient collection and technological difficulties, commercial recycling of REEs in 2001 was still particularly low with less than 1% of the REEs being recycled [4, 5].

Recently, considerable progress has been made in the research of recycling REEs from NdFeB magnets. Demagnetized hydride alloy powder was produced by means of atmospheric pressure hydrogen to separate REE magnets from computer hard disk drives [6, 7]. In order to obtain full conversion of the metal into the oxides, the powder was applied into a grinding and roasting process, from which a fraction (<400 μm) was used in the leaching process. The REEs can then be leached from the powder by mineral acids such as HCl, HNO_3 , and H_2SO_4 . The major components in the leaching solution are Nd, Co and Dy. With the selective leaching, iron (Fe) is left in the solid residue [8, 9].

For several decades, ion exchange has received growing attention in various industries for solution purification by removal of the targeted dissolved ions [10]. α -zirconium phosphate ($\text{Zr}(\text{HPO}_4)_2 \cdot \text{H}_2\text{O}$, α -ZrP), one form of the crystalline acid salts of zirconium, has been extensively studied for applications in catalysis [11], radionuclide removal [12], artificial kidneys [13], and as proton conductors in full cells [14]. Crystalline α -ZrP was first synthesized in 1964 by refluxing an amorphous ZrP gel in phosphoric acid [15]. Since then, synthesis of ZrP with different structures, ion exchange properties, particle sizes, structures, and morphologies have been systematically investigated [16–19]. However, very little is known regarding its ion exchange behaviors toward REE ions.

In this paper, the fundamental ion exchange properties of α -ZrP were studied for Nd, Dy, and Co ions with a view of separation and recycling NdFeB magnets. The study included the synthesis and characterization of the α -ZrP material as well as the determination of its acidity, selectivity, and loading response to different pH values for the metal ions. The kinetic mechanism of the material for the metal ion uptakes was elucidated, too. Moreover, the mechanism of uptake in the α -ZrP structure is also explained. Finally, preliminary batch stripping using mineral acids was investigated.

Experimental

Chemicals

Zirconyl chloride octahydrate (98%), hydrochloride (36%), sodium phosphate monobasic monohydrate (99.8%), and phosphoric acid (85%) were used for the material synthesis. Cobalt nitrate hexahydrate (98%), neodymium nitrate hexahydrate (99%), dysprosium nitrate hydrate (99%),

sulfuric acid (95–97%), nitric acid (67–69%), hydrochloride (36%), and phosphoric acid (85%) were used in the ion exchange experiments. All chemicals were purchased from Sigma-Aldrich except for sulfuric acid from J. T. Baker and used without further purification.

Instrumentation and Analysis Methods

X-ray powder diffraction (XRD) patterns were recorded by a Philips PW3710 X-ray powder diffractometer with the working conditions: 40 kV, 30 mA, Cu- K_α radiation. Fourier transform infrared (FT-IR) spectra were recorded on a Perkin Elmer Spectrum one FT-IR spectrometer. Thermogravimetry (TG) was performed on a Mettler Toledo TGA850 in flowing N_2 gas with a heating rate of $10^\circ\text{C min}^{-1}$. Scanning electron microscope (SEM) images were collected using a Hitachi Hi-Tech S-4800 FESEM. A microwave plasma-atomic emission spectrometer (MP-AES) Agilent 4100 was used for analysis of metal ions. A digital pH meter (Orion model 920A) was used for the pH measurements.

Synthesis of α -ZrP

α -ZrP was synthesized using the reflux method and adapted modifications based on gamma ZrP described by Rajeh and Sziertes [24]. Solution A was prepared by dissolving 322.25 g of $\text{ZrOCl}_2 \cdot 8\text{H}_2\text{O}$ in 300 mL of water in a 3 L glass Huber-reactor. The solution inside the reactor was stirred constantly with a mechanical motorized stirrer (100 rpm), while its temperature was maintained at $80 \pm 1^\circ\text{C}$. Subsequently, solution B (828.18 g of $\text{NaH}_2\text{PO}_4 \cdot \text{H}_2\text{O}$ in 600 mL of 3 M HCl) was added dropwise to the reactor. A white precipitate was obtained after the addition of solution B and the reaction mixture was left to reflux at the same temperature for 24 h, and cooled to room temperature for another 24 h. Then, the precipitate was washed sequentially with 3 L of 2.0 M HCl and 2 L of 2.0 M H_3PO_4 to remove the unbound Na^+ and Cl^- ions. Finally, the product was rinsed with deionized water until it was at pH 3, and dried in an oven at 65°C . The dried product was ground and sieved to 75–152 μm (200–100 mesh) grain size. The as-prepared α -ZrP was equilibrated with 0.1 M HNO_3 (the solid/liquid ratio was 1 g/20 ml) by a rotating mixer for 1 day. The pretreated α -ZrP was washed by deionized water until it was at pH 3.

Preparation of Ternary Co–Nd–Dy Solution

The ternary mixture of Co, Nd, and Dy was prepared by mixing $\text{Co}(\text{NO}_3)_2 \cdot 6\text{H}_2\text{O}$, $\text{N}_3\text{NdO}_9 \cdot 6\text{H}_2\text{O}$, and $\text{DyN}_3\text{O}_9 \cdot \text{XH}_2\text{O}$ into samples of different pH values, HNO_3 with the molar proportion of $\text{Co(II)}:\text{Nd(III)}:\text{Dy(III)} = 1:1:1$. The

solutions with concentrations from 0.01 to 10 mM were prepared at pH values of approximately 3 and 5.

pH Titration Studies

To obtain the pH titration curve, 100 mg of α -ZrP was placed in 19 mL of 1.0 M NaNO₃ solution and titrated with different amounts (250–1050 μ L) of 1 M NaOH solution. The samples were equilibrated for 24 h in a rotary mixer (60 rpm), and then their pH values were measured after phase separation by centrifugation at room temperature (23 °C).

Effect of pH on Sorption

Investigations of the effect of solution pH on Co(II), Nd(III), and Dy(III) sorption (distribution coefficient K_d) were conducted in 1 and 2 mM ternary solutions, using pH values selected from a range of 1 to 6 after checking the solubility product K_{sp} of Co(OH)₂, Nd(OH)₃ and Dy(OH)₃. 100 mg of α -ZrP was placed into each 20 mL polyethylene vial filled with 20 mL of 1 or 2 mM equimolar Co(II), Nd(III), and Dy(III) at different pHs (1–6), respectively. After 6 h, the pH value of each vial was checked and readjusted when necessary with 1 M NaOH. The vials were then equilibrated for 3 d in a rotary mixer (60 rpm). Finally, the vials were centrifuged for 15 min at 4000 rpm, and the supernatants were separated for pH and metal measurements with MP-AES.

Sorption Kinetic Studies

Sorption kinetics tests were performed using various reaction times (from 0.25 to 72 h). For each experiment, 100 mg of α -ZrP was added to 20 mL polyethylene vials with 20 mL of 1 mM equimolar Co(II), Nd(III), and Dy(III) solutions, respectively. The kinetic results were obtained by assaying the sample contents with MP-AES.

Isotherm Studies

100 mg of α -ZrP was equilibrated for 3 d with 20 mL of each ternary Co–Nd–Dy solution (0.01–10 mM with an adequate interval) at pH 2.7 or 4.5 in a rotary mixer (60 rpm). The phase separation was done by centrifugation as described above, and the Co(II), Nd(III), and Dy(III) concentrations of the supernatants were determined with MP-AES.

Batch elution Studies

For each experiment, 100 mg of α -ZrP was added to polyethylene vials and loaded with 20 mL of 10 mM equimolar Co(II), Nd(III), and Dy(III) solutions, and the

vials rotated for 3 d. Then the supernatants were separated from the solids for measurements by centrifugation for 15 min at 4000 rpm. The remaining solids in the vials were washed three times with deionized water and dried overnight at 60 °C. After that, 20 mL of 0.1, 0.3 and 1 M HCl, HNO₃, H₃PO₄ and H₂SO₄ eluents were added, respectively, to each vial followed by 3 d rotation. The supernatants were separated by centrifugation for measurements. The remaining solids were also washed three times with water and then dried for XRD analysis.

Column Loading/Elution Experiments

Column tests were performed in a Bio-Rad glass column with an inner diameter of 10 mm and a height of 100 mm at room temperature (22–23 °C). The columns were filled with α -ZrP material which was carefully packed up to 5.5 cm in the columns. A ternary Co–Dy–Nd solution with a pH value of 2.5 and equimolar of 1.0, 0.5 and 0.1 mM was prepared as the feed solution. The loading process was carried out at a speed of two bed volumes (BV) per hour. Then the pH 2.5 nitric acid was loaded as the washing agent using 6 BV at 2 BV/h. After this the stripping process was started using 0.3 M HNO₃ as the stripping agent at a stripping speed of 1 BV/h. Finally, the samples were collected for MP-AES measurement. The following experiments used the same process, and the only change was the use of two different mixed stripping agents 0.5 M HNO₃ and 0.1 M H₃PO₄ (volume ratio = 1:1) or 0.3 M HNO₃ and 0.1 M H₃PO₄ (volume ratio = 1:1).

Theoretical Background

The distribution coefficient (K_d) describes the distribution of solute ions between the solution and the ion exchanger. It can be calculated from solution phase measurements of A by

$$K_d = \frac{[A_0] - [A_{eq}]}{[A_{eq}]} \times \frac{V}{m} \quad (1)$$

where $[A_0]$ is the solution concentration of A initially, $[A_{eq}]$ is the corresponding concentration at equilibrium, V is the volume of solution, and m is the mass of exchanger material.

When considering the exchange of metal ions M^{n+} for hydronium ions H^+ , the selectivity coefficient $k_{M/H}$ becomes

$$k_{M/H} = \frac{[\overline{M}][H]^n}{[M][\overline{H}]^n}, \quad (2)$$

where $[\overline{M}]/[M]$ is the distribution coefficient (K_d) for ion M. In the cases where metal loading in exchanger is low in the system ($[\overline{M}] \ll [\overline{H}] \approx Q$ and $[M] \ll [H]$)

$$\log K_d = \log\left(k_{\frac{M}{H}}Q^n\right) - n \log[H] = \log\left(k_{\frac{M}{H}}Q^n\right) + npH \quad (3)$$

In other words, $\log K_d$ is linear as a function of pH with a slope of $+n$. Here, Q is the total capacity of the ion exchanger.

In practical sorption studies, simpler terminology is often used instead of the rigorous equations given above, especially when the sorption mechanism and system are unknown. For instance,

$$[\overline{M}] = q_{eq} \quad (4)$$

$$[M] = C_{eq} \quad (5)$$

where q_{eq} is the solute concentration in the sorbent phase at equilibrium, C_{eq} is the metal concentration in the batch stripping solution at equilibrium. Solid phase concentrations are often measured from the changes of solution phase concentrations as concentration measurements are generally more accurate than solid phase measurements. Thus,

$$[\overline{M}] = (C_0 - C_{eq}) \times \frac{V}{m} \quad (6)$$

$$[\overline{H}] = Q - n[\overline{M}] \quad (7)$$

In this work, metal concentrations were determined via the solution concentrations as described by Eqs. 6 and 7.

Rational concentrations (e.g. equivalent fractions) or mole fractions are often used instead of molarities or molalities. For instance, the equivalent fraction of M^{n+} in the sorbent

$$\overline{E}_M = \frac{Z_M q_M}{Q} \quad (8)$$

where Z_M , q_M and Q are M ion's charge, equilibrium concentration in the sorbent (mM/g), and the capacity of the ion exchanger (meq/g), respectively.

Results and Discussion

Structural Characterization

The crystalline α -ZrP has a layered structure (Fig. 1a) which is formed by zirconium atoms connected through the oxygen atoms of the phosphate groups. Three oxygen atoms of each phosphate group contributes to three different zirconium atoms, so a distorted equilateral triangle is formed by this structure. The OH^- group in this structure is embedded in the interlayer space. The XRD pattern of the synthesized material can be seen in Fig. 1b and it closely resembles the XRD patterns of α -ZrP. The first peak shows a d -spacing of 7.56 Å, which corresponds to the interlayer distance between the 002 planes of crystalline α -ZrP [12].

Figure 1c, d show the SEM images of the synthesized α -ZrP with a regular planar size and nearly hexagonal shape. The length dimension of the crystalline α -ZrP platelet varies from 1 to 4 μm , which is as long as the length of that prepared by the HF method, and larger than those of the hydrothermal and refluxing methods (see Table 1) [20–22]. The elimination of HF as a toxic solvent in the synthesis is in line with the aims of green chemistry. The reaction temperature is also lower than in other reported methods. Our method could be easily scaled-up and is potentially promising for future industrial application.

FTIR Spectroscopy and Thermogravimetric Analysis

The FTIR spectroscopy of crystalline α -ZrP (Fig. 2a) shows bands at 3593, 3510, 3148, and 1618 cm^{-1} that can be ascribed to the stretching and bending of the lattice water. The bands at wavenumbers 1249, 1069, 1038 and 963 cm^{-1} belong to P-OH deformation and vibration of the orthophosphate group [23]. The TGA curves of crystalline α -ZrP (Fig. 2b) show the first endothermic process to be from 25 to 110 °C that is characterized by water loosely adsorbed on the surface of the ZrP crystals and interlayer water. The second process (from 110 to 360 °C) belongs to the loss of strongly bound crystalline water. The third stage (from 360 to 900 °C) could be attributed to the loss of structural water originated at the decomposition of phosphate groups [24]. From 110 up to 900 °C, the total weight loss of crystalline α -ZrP is 10.96%, which corresponds to the loss of two water molecules leading to formation of pyrophosphate ZrP_2O_7 . After calculation we obtained the formula of crystalline α -ZrP which is $Zr(HPO_4)_2 \cdot 1.012H_2O$. These results combined with the FT-IR and XRD results proved the success of the synthesis of crystalline α -ZrP.

Titration for the Ion Exchange Characterization

Like phosphoric acid, zirconium phosphate is weakly acidic in nature, and the dissociation of the OH^- groups attached to the phosphorous atom can be characterized by the dissociation constant K_a :

$$\frac{[PO^-][H^+]}{[POH]} = K_a \quad (9)$$

and

$$pK_a = -\log K_a \quad (10)$$

where [POH] is the concentration (mM/g) of undissociated phosphorous OH^- groups in the material and $[PO^-]$ is that of the dissociated ones. $[H^+]$ refers to hydronium ion

Fig. 1 **a** Polyhedral representation of the structure of crystalline α -ZrP. **b** X-ray powder diffraction pattern of the synthesized α -ZrP. **c, d** SEM images of the crystalline α -ZrP (Color figure online)

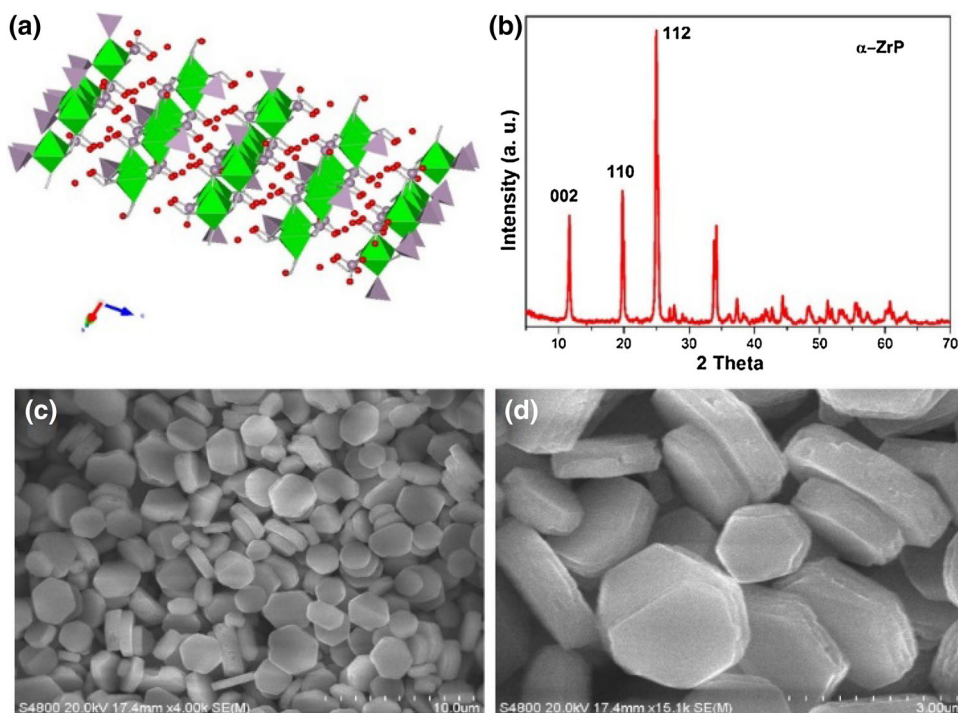


Table 1 Data for pertinent crystalline α -ZrP synthesized by different methods

Synthesis method	Zr source	P source	Temperature	Reaction time	Average diameter	Time (year)	References
Hydrothermal method	ZrOCl ₂ ·8H ₂ O	3 M H ₃ PO ₄	200 °C	24 h	~400 nm	2006	[20]
	ZrOCl ₂ ·8H ₂ O	12 M H ₃ PO ₄	200 °C	24 h	1 μm	2006	[20]
	ZrOCl ₂ ·8H ₂ O	3 M H ₃ PO ₄ , 5 M HF	100 °C	24 h	1–4 μm	2006	[20]
Refluxing method	ZrOCl ₂ ·8H ₂ O	3 M H ₃ PO ₄	100 °C	24 h	~60 nm	2006	[20]
	ZrOCl ₂ ·8H ₂ O	12 M H ₃ PO ₄	100 °C	24 h	~200 nm	2006	[20]
	ZrOCl ₂ ·8H ₂ O	6 M H ₃ PO ₄	94 °C	48 h	~120 nm	2014	[21]
	ZrOCl ₂ ·8H ₂ O	10 M H ₃ PO ₄	–	–	250 nm	2000	[22]
	ZrOCl ₂ ·8H ₂ O	NaH ₂ PO ₄ ·H ₂ O, 3 M HCl	80 °C	24 h	1–4 μm	2015	This study

concentration in the pore water inside the pores of the solid material and may not necessarily be that of the external solution [25].

The degree of dissociation (β)

$$\beta = \frac{[\text{PO}^-]}{[\text{POH}] + [\text{PO}^-]} \quad (11)$$

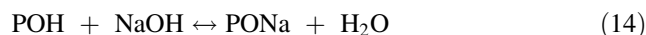
depends on $\text{p}K_a$ and pH according to

$$\log \frac{1-\beta}{\beta} = \text{p}K_a - \text{pH} \quad (12)$$

Here, pH is obtained by solving Eq. 12 for β yields

$$\beta = \frac{1}{1 + \frac{[\text{H}^+]}{K}} = \frac{1}{1 + 10^{\text{p}K_a - \text{pH}}} \quad (13)$$

After titration with NaOH, the charge of the PO^- groups in the material will be balanced by the Na^+ ions:



The total ion exchange capacity (Q) of the material is thus

$$Q = [\text{POH}] + [\text{PONa}] \quad (15)$$

Based on Eq. 14, the conversion to the Na form (q_{Na} , mmol/g) can be calculated from

$$q_{\text{Na}} = \left([\text{OH}^-]_i - [\text{OH}^-]_{\text{eq}} \right) (V/m) \quad (16)$$

where $[\text{OH}^-]_i$ is the initial concentration of $[\text{OH}^-]$ in the solution, $[\text{OH}^-]_{\text{eq}}$ is the concentration of $[\text{OH}^-]$ in the

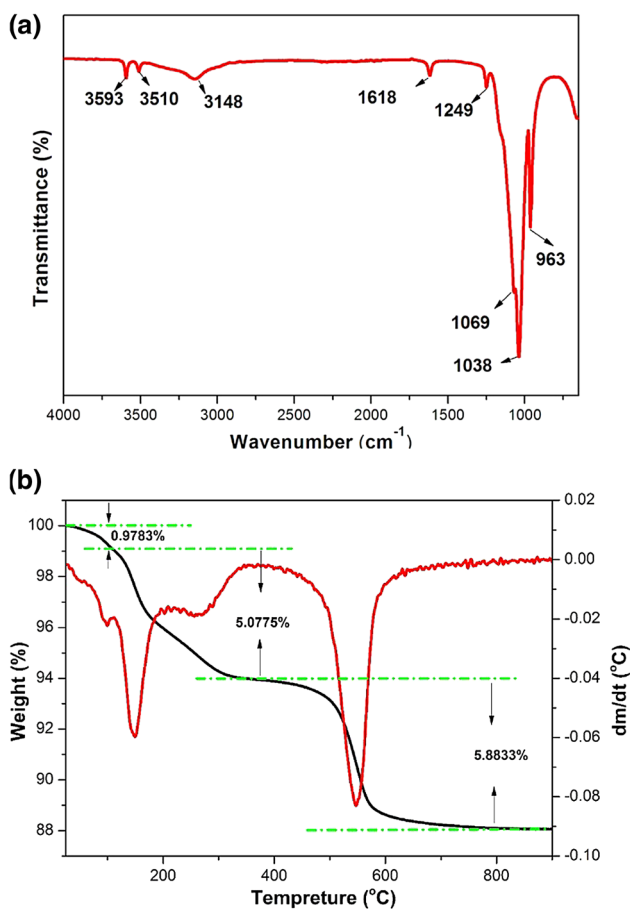


Fig. 2 **a** FT-IR spectrum of crystalline α -ZrP. **b** TGA of crystalline α -ZrP in nitrogen atmosphere at a heating rate of 10 °C/min (Color figure online)

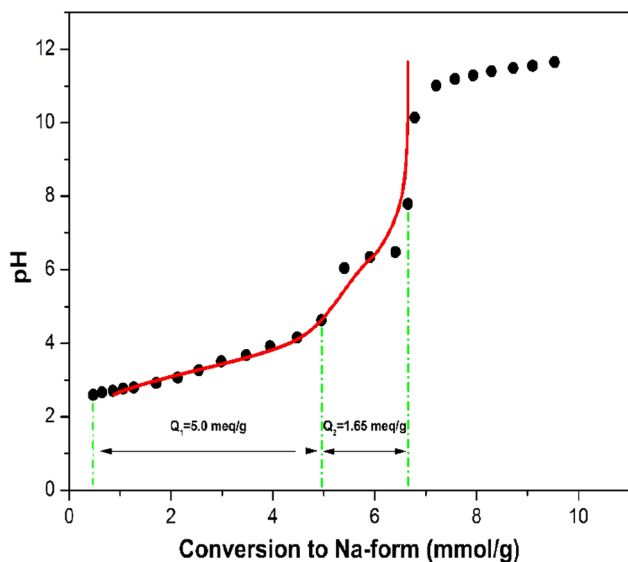


Fig. 3 Titration of crystalline α -ZrP with NaOH in 1.0 M NaNO_3 solution. Observed conversion to Na form in titration (Eq. 10, filled circle), calculated conversion using Eq. 11 (solid line) with $\text{p}K_{a1} = 3.3$ and $\text{p}K_{a2} = 6.3$ (Color figure online)

equilibrium state, V is the volume of solution, and m is the mass of material.

However, when immersed in the 1.0 M NaNO_3 solution, some conversion of ZrP material to the Na form takes place by the reaction



This was evident from the observation that when ZrP (0.1 g) equilibrated in 1.0 M NaNO_3 (19 mL), the pH of the solution decreased from 6.50 to 2.60. Thus, based on Eqs. 14 and 17, the conversion to the Na form should be calculated from

$$q_{\text{Na}} = \left([\text{OH}^-]_i - [\text{OH}^-]_{\text{eq}} + [\text{H}^+]_{\text{eq}} - [\text{H}^+]_i \right) (V/m) \quad (18)$$

where $[\text{H}^+]_i$ is the initial concentration of $[\text{H}^+]$ in the solution, and $[\text{H}^+]_{\text{eq}}$ is the concentration of $[\text{H}^+]$ in the equilibrium state.

Earlier studies have shown that the titration behavior of ZrP depends strongly on the preparation method and on the crystallinity of the material [26, 27]. Generally, materials with a low degree of crystallinity have steadily rising titration curves with no clear inflections points. As the crystallinity increases, equivalence points appear and become sharper with the increasing crystallinity. Titration of highly crystalline ZrP with NaOH indicated it is a diprotic weakly acidic cation exchanger with a total ion exchange capacity of about 6.6 meq/g [28]. This can be readily rationalized from its chemical formula $\text{Zr}(\text{HPO}_4)_2$. When LiOH was used, however, the behavior was not clearly diprotic, as the amounts of OH-groups corresponding to the first and second deprotonations were not equal [27, 29]. Also, the cation present has a strong effect on the titration curve as the amount of ZrP for the affinity varies for the different cations [14, 18, 19]. While numerous titration studies have been carried out for ZrP materials, there seems to be no numeric data on their $\text{p}K_a$ values.

The titration curve obtained for the ZrP in this study showed a diprotic character with the first equivalence point at Na-loading of about 5 meq/g (Fig. 3). The second equivalence point appeared at 6.6 meq/g, which is in good agreement with the total ion exchange capacity observed in earlier studies [14, 18–20]. The shape of the titration curve thus very closely resembled the one obtained in an earlier study using LiOH as titrant [18, 20]. Because of this, it was not possible to use the conventional theory of diprotic acids to describe the acidity of the ZrP material. Instead, based on the observed equivalence points it was assumed that the ion exchange capacity of the more acidic sites ($\text{p}K_{a1}$) was 5.0 meq/g (Q_1) which left 1.65 meq/g (Q_2) for the lesser sites ($\text{p}K_{a2}$). The $\text{p}K_a$ -values were tentatively chosen from the middle of the plateaus of the titration curve ($\text{p}K_{a1} = 3.5$, $\text{p}K_{a2} = 6.5$). The degree of dissociation was

Table 2 Parameters for Co(II), Nd(III), and Dy(III) sorptions from linear fitting

pH range	Linear fit of Co(II)			Linear fit of Dy(III)			Linear fit of Nd(III)		
	Slope	Intercept	R^2	Slope	Intercept	R^2	Slope	Intercept	R^2
1.0–5.3	0.3398	0.2992	0.9946	0.5479	0.4079	0.9997	0.587	0.471	0.9992
5.3–6.3	2.3584	−10.285	0.9999	2.253	−8.6107	0.9999	2.416	−9.3014	0.9998

then calculated simultaneously for both sites using Eq. 13 at different pH values and converted to Na loading (q_{Na}) by

$$q_{\text{Na}} = \beta_1 Q_1 + \beta_2 Q_2 \quad (19)$$

The best fit between the observed (q_{Na} calculated from pH measurements using Eq. 18) and the calculated Na conversions (Eq. 19) was obtained using $\text{p}K_{\text{a}1} = 3.3$ and $\text{p}K_{\text{a}2} = 6.3$ (Fig. 3).

Effect of pH on Sorption

In the ternary 1 mM solution, the uptakes of REEs and Co were low (<0.1 meq/g) when the pH was <2.7 but increased very strongly thereafter until uptakes reached a plateau at approximately pH 3.5 (Fig. 4a, i). The strong increase in the uptakes was consistent with the determined $\text{p}K_{\text{a}1}$ value of 3.3. Maximum uptake values for Co, Dy, and Nd were 0.435, 0.609, and 0.627 meq/g, respectively, totaling 1.67 meq/g. At pHs > 3.5 practically all REE and Co were removed from the solution. The strong increase of metal uptakes was clearly evident in the K_{d} values that increased four orders of magnitude at approximately pH 3.5 (Fig. 4a, ii).

In the case of 2 mM solutions (Fig. 4b, i–ii) the situation was somewhat different: no plateaus were observed in the uptake curves. This was obviously due to the increasing uptake of Co and REEs by the second, less acidic exchange site ($\text{p}K_{\text{a}2}$). Metal uptakes still increased above pH 6.3 being 1.11 meq/g for Nd, 1.10 meq/g for Dy, and 0.78 meq/g for Co, totaling 2.99 meq/g, which was a 79% increase compared to the 1 mM solution.

This concept is supported by the K_{d} -data (Fig. 4c, d) which shows two linear domains. The first domain, at pH 1–5.3, $\log K_{\text{d}}$ versus pH has a low gradient: slope 0.33–0.59. For the second domain at pH 5.3–6.4 (Table 2), the gradient of $\log K_{\text{d}}$ increases considerably: slope 2.25–2.42 (Table 2). Evidently, the second domain corresponds to REE and Co uptake on the less acidic exchange site with $\text{p}K_{\text{a}2} = 6.3$. In the second domain, the slopes of $\log K_{\text{d}}$ are between the theoretical slopes (Eq. 3) of +2 (Co) and +3 (Nd, Dy).

Adsorption Kinetics

In order to investigate the sorption mechanism of crystalline α -ZrP, characteristic constants of sorption were determined using a pseudo-first-order equation, pseudo-

second-order equation, and simplified model of resistance to intraparticle diffusion [30–32].

In the pseudo-first-order equation

$$\log(q_e - q_t) = \log q_e - \left(\frac{k_1}{2.303}\right)t \quad (20)$$

and in the pseudo-second-order equation

$$\frac{t}{q_t} = \frac{1}{k_2 q_e^2} + \frac{1}{q_e} t \quad (21)$$

where q_e is the solute concentration in the sorbent phase at equilibrium, q_t is the solute concentration in the sorbent phase at any given time t , and k_1 and k_2 are the rate constants of the pseudo-first-order and pseudo-second-order kinetic models, respectively. Intraparticle diffusion can thus be expressed

$$q_t = k_{\text{int}} t^{1/2} + C \quad (22)$$

where k_{int} is the intraparticle diffusion constant. A plot of q_t versus $t^{1/2}$ should be a straight line with a slope K_{int} and intercept C when the adsorption mechanism follows the intraparticle diffusion process.

The exchange rates of Co(II), Nd(III), and Dy(III) were studied in individual solutions with pH values of 2.5, and the liquid volume/ion exchange mass ratio was kept at 20 mL/0.1 mg. The uptakes for Co(II), Nd(III), and Dy(III) increased with the increasing time from 0 to 24 h, when equilibrium is almost reached (Fig. 5a). A time period of 72 h was observed to be adequate for the three metal ions to reach equilibrium.

From the parameters of the fitted models (Table 3), it can be seen that the pseudo-second-order model gives the best fits for the kinetic profiles for the sorption of Co(II), Nd(III), and Dy(III) ions onto crystalline α -ZrP particles with correlation coefficients $R = 0.999$. The pseudo-first-order model and intraparticle diffusion model gave clearly much lower R values. The pseudo-second-order model is based on the assumption that the rate-limiting step may be chemical sorption [33]. In our experiment, sorption appears to be ion exchange process between H^+ and Co^{2+} , Nd^{3+} and Dy^{3+} .

Sorption Isotherms and Thermodynamics

Sorption isotherms were determined at equilibrium pH values around 2.5 (Fig. 6a) and 4.5 (Fig. 6b). At pH 2.5 the

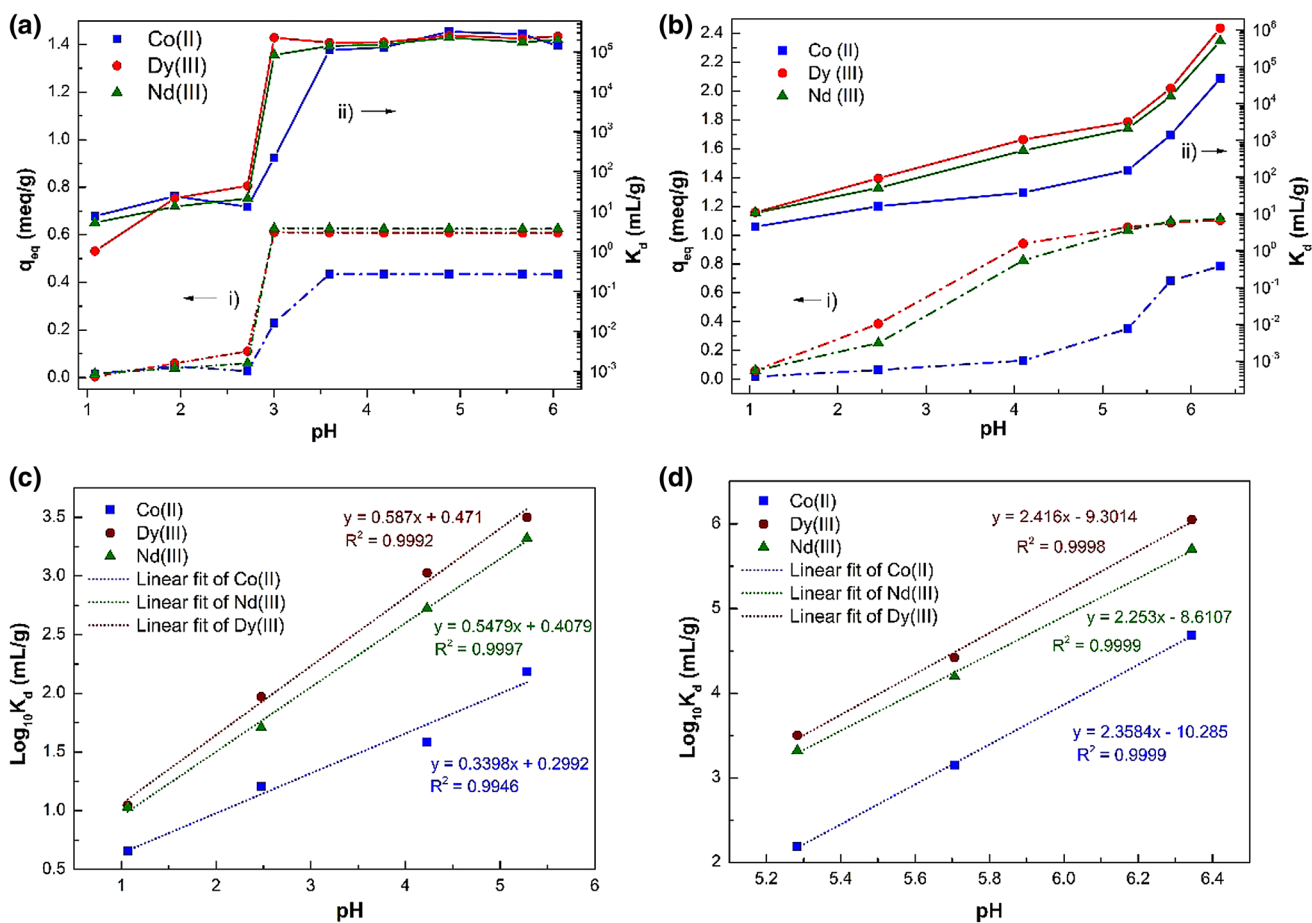


Fig. 4 The effects of pH on the sorptions of Co(II), Nd(III), and Dy(III) nitric acid solution with the initial concentrations of 1 mM by α -ZrP: **a** (i) the metal loading curves, (ii) distribution coefficients. The effects of pH on the sorptions of Co(II), Nd(III), and Dy(III) nitric

acid solution with initial concentrations of 2 mM by α -ZrP: **b** (i) the metal loading curves, (ii) distribution coefficients. **c** Linear fitting of $\log K_d$ over pH 1.0–5.3. **d** Linear fitting of $\log K_d$ over pH 5.3–6.3 (Color figure online)

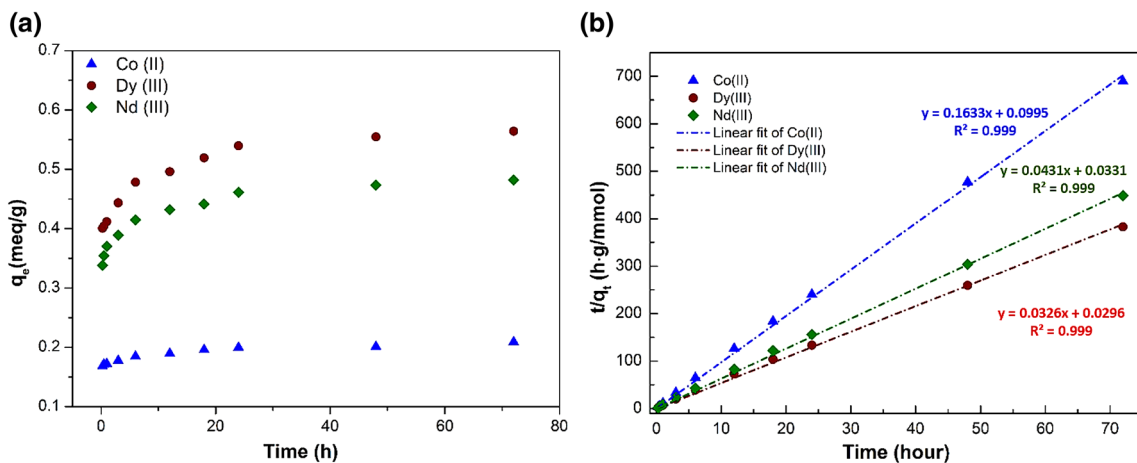


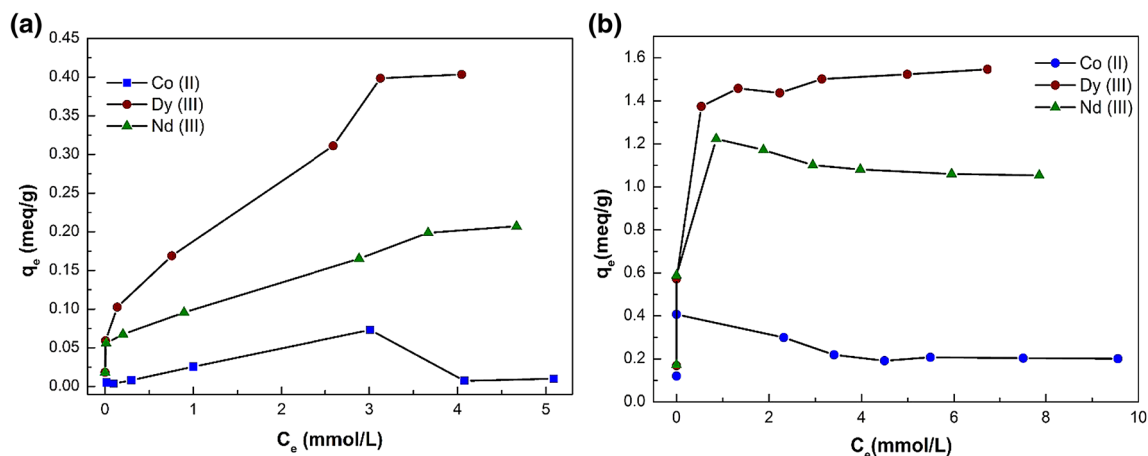
Fig. 5 **a** The effects of contact time on the sorption kinetics of 1 mM nitric acid solutions of Co(II), Nd(III), and Dy(III) onto crystalline α -ZrP ($pH_{eq} \sim 2.7$). **b** Pseudo-second-order sorption model fitting of Co(II), Nd(III), and Dy(III) onto crystalline α -ZrP (Color figure online)

metal uptakes increased with the increasing metal solution concentration (c_e) until a concentration of about 3 mM (Fig. 6a). At higher c_e , Nd and Dy uptakes increased but

Co uptake decreased which is apparently due to the desorption and replacement of Co by Nd and Dy. At c_e of approximately 4 mM, the uptakes were 0.18 meq/g for Nd,

Table 3 Fitted pseudo-first-order, pseudo-second-order, and particle diffusion kinetic model parameters for Co(II), Nd(III), and Dy(III) sorption

Metal ion	$q_{\max, \text{exp.}}$ (mmol g ⁻¹)	Pseudo-first-order kinetics			Pseudo-second-order kinetics			Intraparticle diffusion		
		k_1 (h ⁻¹)	q_{eq} (mmol g ⁻¹)	R^2	k_2 (mg g ⁻¹ h ⁻¹)	q_{eq} (mmol g ⁻¹)	R^2	C (mg.g ⁻¹)	K_{int} (mmol g ⁻¹ h ^{-1/2})	R^2
Co(II)	0.104	0.037	0.0167	0.961	0.268	0.104	0.999	0.085	0.00256	0.937
Dy(III)	0.188	0.062	0.0505	0.976	0.036	0.188	0.999	0.927	0.00749	0.927
Nd(III)	0.161	0.059	0.0380	0.963	0.056	0.161	0.999	0.896	0.00590	0.896

**Fig. 6** The isothermal sorption curves of Co(II), Nd(III), and Dy(III) from a nitric acid solution by crystalline α -ZrP at **a** $\text{pH}_{\text{eq}} \sim 2.5$ and **b** $\text{pH}_{\text{eq}} \sim 4.5$ (Color figure online)

0.40 meq/g for Dy, and only 0.02 meq/g for Co. The proportion of Co(II) uptake was thus around 3.3 equivalent-% of the total metal uptake. This could be explained qualitatively by the preference of ion exchangers for ions of higher valence. However, there was also a striking difference in Nd and Dy uptakes that was not evident in the pH response experiments (Fig. 4a–b). At pH 4.5 both Co and Nd uptakes started to decrease before the c_e reached 2 mM (Fig. 6b), clearly by desorption of Dy which had an increasing uptake over the whole c_e range studied. At a c_e of approximately 7 mM, the uptakes were 1.1 meq/g for Nd, 1.5 meq/g for Dy, and only 0.24 meq/g for Co, totaling 2.84 meq/g. At a c_e of about 7 mM, the proportion of Co(II) uptake was around 8.4 equivalent-% of the total metal uptake. Again, there was a large difference in the Nd and Dy uptakes which may imply there are interesting opportunities for the separation of Nd from Dy.

The binary selectivity coefficients calculated from the isotherms at pH 4.5 (Fig. 7) showed that $k_{\text{Co/H}}$ was practically a constant of approximately 1.5×10^{-8} . For Nd and Dy, the selectivity coefficients increased with the increasing equivalent fraction in the solid from about 10^{-13} to 10^{-11} . The values seem very low considering that the trivalent Nd and Dy were highly preferred over the divalent Co by the α -ZrP. Obviously, the formalism of the equation

for the selectivity coefficient (Eq. 2) can give rise to considerable variation as the value is dependent on the second (Co) or third (Nd, Dy) power of the hydronium ion concentration in solution.

Batch Elution Studies

In the batch stripping experiments, the percentages of stripping and distribution coefficient K_d at stripping were determined. The percent stripping (Strip %) was calculated from

$$\text{Strip \%} = \left(\frac{c_{\text{eq}}}{q_i} \times \frac{V}{m} \right) \times 100 \quad (23)$$

where q_i is the initial amount of M loaded in the sorbent, and C_{eq} is metal concentration in the batch stripping solution at equilibrium. The K_d was determined from the relation

$$K_d = \frac{q_{\text{eq}}}{c_{\text{eq}}} = \frac{q_i - c_{\text{eq}}}{c_{\text{eq}}} \times \frac{V}{m} \quad (24)$$

The symbols are the same as those in Eq. 23.

In terms of Strip %, 0.1 M H₂SO₄ displayed the best results in removing 96.7% of Dy(III) and 99.1% of Nd(III) (Fig. 8). The removal of metals decreased with the increasing H₂SO₄ concentration. Nitric and hydrochloric

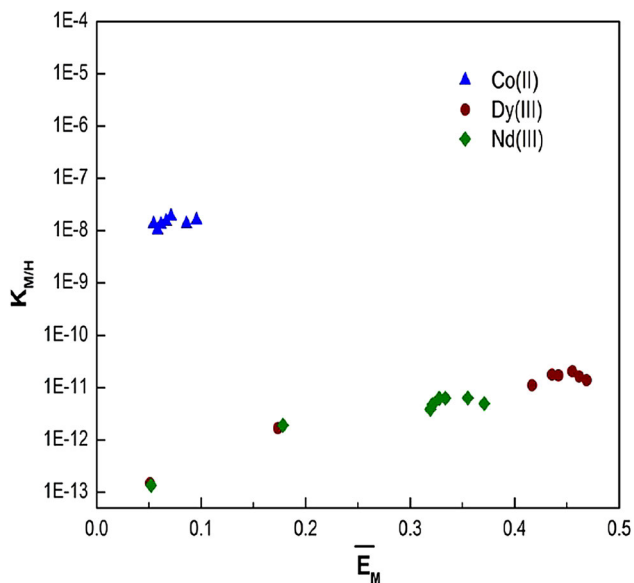


Fig. 7 The effects of the binary selectivity coefficient $K_{M/H}$ \bar{E}_M ($M = \text{Co(II)}$, Dy(III) , or Nd(III)) on the isothermal sorption from 0.3 to 10 mM ($\text{pH}_{\text{eq}} \sim 4.5$) of Co(II) , Nd(III) , and Dy(III) nitric acid solution by crystalline $\alpha\text{-ZrP}$ (Color figure online)

acid had 60–70% Nd and Dy stripping at 0.1 M concentration and the Strip % rose to 90% and higher at 1 M concentration (Fig. 8). Theoretically, K_d at stripping (Table 4) can be used to estimate the amount of stripping agent (ml/g of $\alpha\text{-ZrP}$) needed for metal elution. Also, the ratio of K_d for two metals can be used to estimate their separation factor (SF). In most cases, the SF(Dy/Nd) is close to unity. For example, with H_2SO_4 as a stripping agent, the SF (Dy/Nd) were calculated to be 1.27, 1.21 and 1.50 when using concentrations of 0.1, 0.3 and 1 M, respectively. However, in case of phosphoric acid, the achieved SF (Dy/Nd) were 0.22, 0.74 and 2.64 when using concentrations of 0.1, 0.3 and 1 M, respectively. The highest SF (Dy/Nd) 0.22 was achieved using 0.1 M H_3PO_4 . The hydrochloric acid would be the choice of preference since the SF (Dy/Nd) is equal to 3.08 when using 1 M HCl stripping agent (Table 4). Nevertheless, HCl was excluded from the column study, due to its highly corrosive and environmental harmful properties.

Nitric acid was studied in more detail over a wider concentration range than other stripping agents (Fig. 9i). The Strip % for Nd and Dy decreased from about 90% to just a few percent when pH increased from 0 to 2.5. For instance, at pH 0.5 the estimated amount (K_d -value in Fig. 9ii) of HNO_3 needed for column elution was about 25 mL/g for Nd and 32 mL/g for Dy.

Figure 10 shows the XRD patterns of synthesized $\alpha\text{-ZrP}$, a sample loaded with Nd and Dy, and a sample after elution by various acids. As seen in Fig. 10, the XRD patterns show that the crystal structure was kept well after loading and the elution cycle.

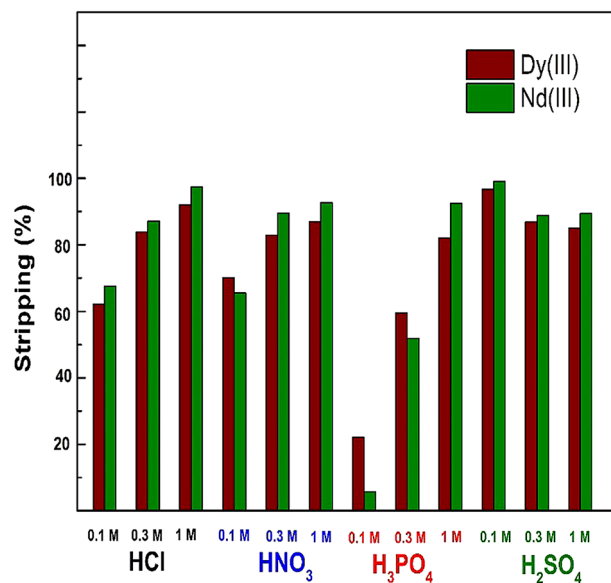


Fig. 8 Batch recovery data for Nd(III) and Dy(III) in different stripping acids (Color figure online)

Table 4 The K_d values and separation factors of the batch recovery data in different stripping acids

Stripping agent		K_d (mL/g)		Separation factor Dy/Nd
		Dy	Nd	
HCl	0.1 M	121	96	1.26
	0.3 M	38	29	1.30
	1 M	17	6	3.08
HNO_3	0.1 M	85	105	0.81
	0.3 M	41	24	1.73
	1 M	30	16	1.91
H_3PO_4	0.1 M	670	3239	0.22
	0.3 M	134	183	0.74
	1 M	43	16	2.64
H_2SO_4	0.1 M	26	21	1.27
	0.3 M	30	25	1.21
	1 M	35	24	1.50

Breakthrough Study

The column loading curves of Co, Nd, and Dy with initial feed concentration of equimolar 1 mM (Fig. 11) at pH 2.5 showed the same uptake pattern that was observed in the isotherm determinations (Fig. 6), i.e. the metals studied were preferred in the order $\text{Dy} > \text{Nd} > \text{Co}$. The loaded amounts of Co(II) , Dy(III) , and Nd(III) were 0.007, 0.114 and 0.072 meq/g, respectively. A total of 0.193 meq/g ions were loaded in fixed bed $\alpha\text{-ZrP}$ at a pH 2.5, which was in line with the value of 0.196 meq/g observed in batch loading at pH 2.7 (Fig. 4a, i). The proportion of Co(II)

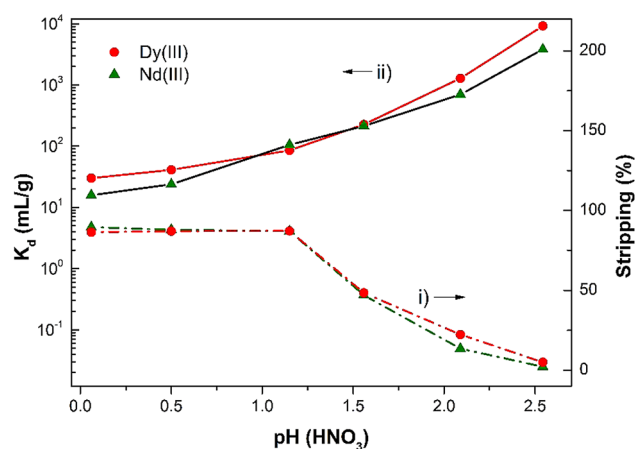


Fig. 9 The stripping percentages (i) and distribution coefficients K_d (ii) of Dy(III) and Nd(III) by crystalline α -ZrP in HNO_3 as a function of pH (Color figure online)

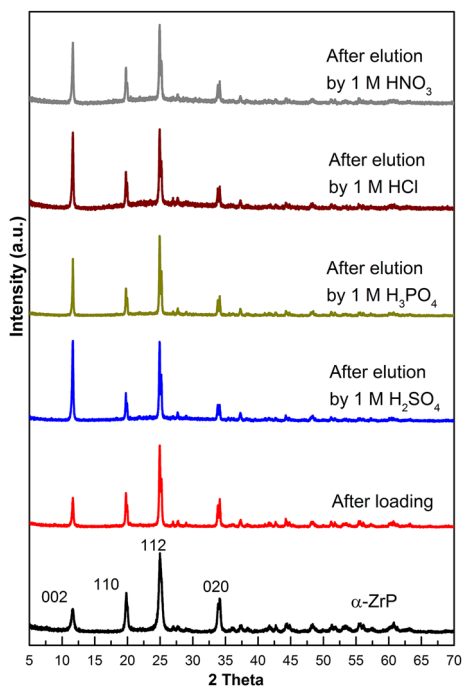


Fig. 10 XRD patterns of α -ZrP, α -ZrP after loading and α -ZrP after elutions by 1 M of H_2SO_4 , H_3PO_4 , HCl , and HNO_3 (Color figure online)

loaded was around 3.7 equivalent-% of the total amount loaded, this also was in conformity with that of 3.3 equivalent-% obtained in batch loading (Fig. 6a).

Stripping Behavior

The column loading curves for Co, Nd, and Dy with an initial feed concentration of equimolar 0.5 mmol/L (Fig. 12a) also showed the same uptake patterns that were observed in the isotherm determinations (Fig. 6) and in the

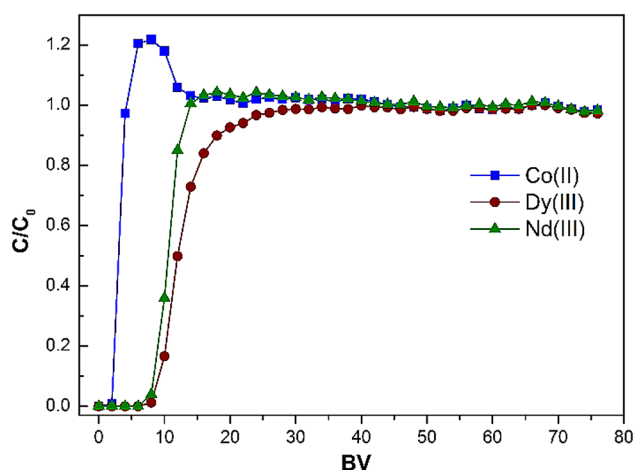


Fig. 11 Breakthrough curves of Co(II), Nd(III), and Dy(III) with initial concentrations of 1 mmol/L in HNO_3 (pH 2.5) (loading speed 2 BV/h) (Color figure online)

breakthrough curves (Fig. 11). The stripping experiments were studied by single acid and acid mixtures. For the stripping curves, the one using 0.3 M HNO_3 as the stripping agent showed modest separation with the average ratio of $[\text{Dy}]/[\text{Nd}]$ in the eluent was approximately 1.5. This ratio is close to what was achieved at the loading stage (Table 5).

Mixed 0.3 M $\text{HNO}_3/0.1$ M H_3PO_4 showed markedly different stripping for Nd and Dy: the ratio of $[\text{Dy}]/[\text{Nd}]$ in eluent is from 3.3 to 7, except in the first fraction the ratio is 1.2. However, the metals did not come out as elution bands because 100% loading did not leave space for the bands to develop in the column. The obvious solution is to use lower degree of metals loading and to use longer columns to allow proper chromatographic separation to take place. This will be the major topic in the next phase of this research.

Conclusions

In this paper, a non-HF synthesis method with a relatively low acid and energy consumption was developed to synthesize a platelet-like highly crystalline inorganic α -ZrP ion exchanger. The ion exchange capacity of the α -ZrP is due to contributions from two acidic sites, one with 5.0 meq/g and another with 1.65 meq/g. The sorption system follows the pseudo-second-order kinetic model. During batch operation, the ZrP materials favor the exchange with trivalent Nd and Dy ions over the divalent Co ions. The loaded REEs were effectively eluted using 0.1 M H_2SO_4 , but there was no Nd/Dy separation. The structure of crystalline α -ZrP was especially well kept after loading and elution in 0.1 and 1 M stripping agents. The column

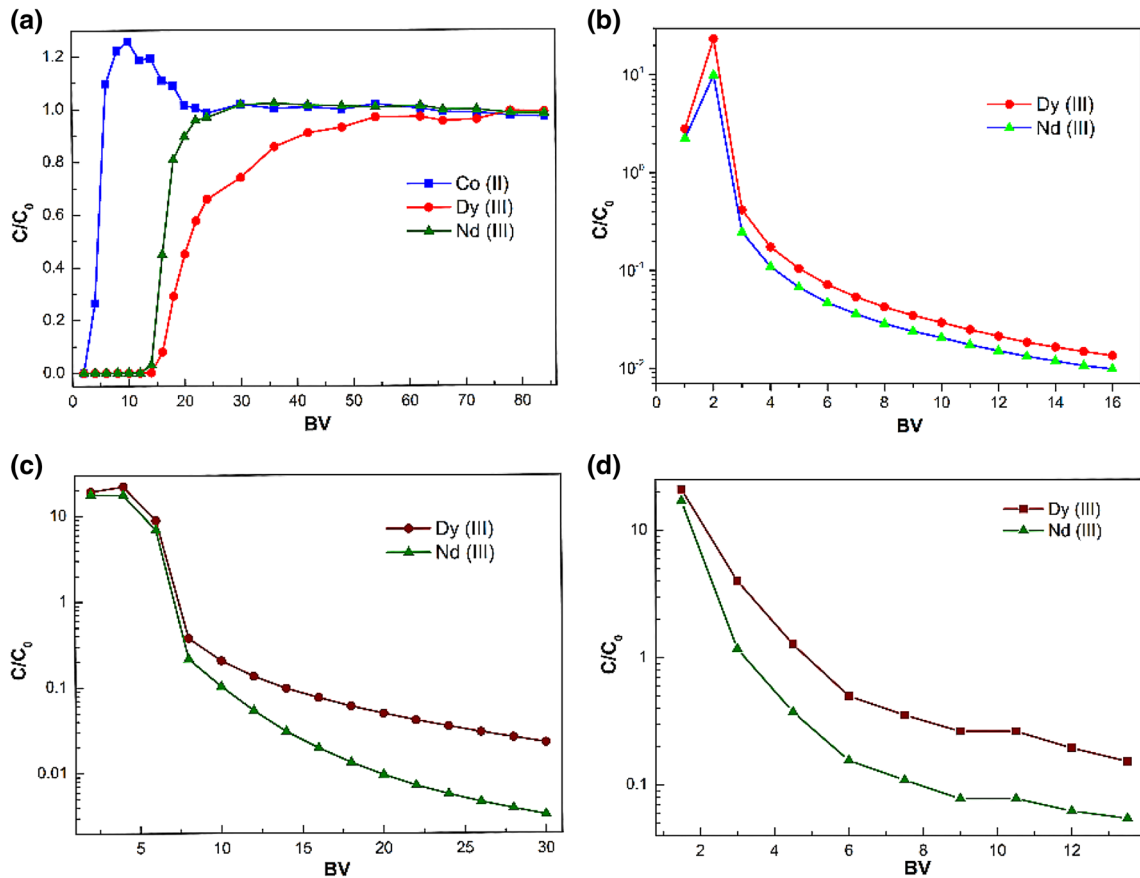


Fig. 12 a Loading curves of Co(II), Nd(III), and Dy(III) with initial concentration of 0.5 mM. Comparison of stripping curves for different stripping agents: b 0.3 M HNO₃, c 0.5 M HNO₃ and

0.1 M H₃PO₄ (volume ratio = 1:1), d 0.3 M HNO₃ and 0.1 M H₃PO₄ (volume ratio = 1:1) (Color figure online)

Table 5 Data of breakthrough experiment with the loading solution of 1 mmol/L of Co(II), Dy(III), and Nd(III) in fixed-bed α-ZrP (1.768 g)

Metal ion	Breakthrough point (BV)	Loaded amount (meq/g)	Equivalent-%	Dy loaded/Nd loaded
Co(II)	2	0.007	3.7	
Dy(III)	8	0.114	59.1	1.58
Nd(III)	8	0.072	37.2	

loading/stripping results were in line with the results of the corresponding batch experiments. The mixed stripping agent 0.3 M HNO₃/0.1 M H₃PO₄ had a separation ratio of around 3.3 for Nd(III) and Dy(III) in the stripping stage, which is promising for future studies. Definitely much more work will be needed to develop a practical column process for Dy/Nd separation.

Acknowledgments The research leading to these results received funding from the European Community’s Seventh Framework Programme ([FP7/2007–2013]) under grant agreement no. 607411 (MC-ITN EREAN: European Rare Earth Magnet Recycling Network, <http://www.erean.eu>). This publication reflects only the authors’ views, exempting the Community from any liability. The authors would like to thank Dr. Rikard Ylmen for his help in drawing the crystal structure.

References

- Binnemans K, Jones PT, Blanpain B, Van Gerven T, Yang Y, Walton A, Buchert M (2013) Recycling of rare earths: a critical review. *J Clean Prod* 51:1–22
- Alonso E, Sherman AM, Wallington TJ, Everson MP, Field FR, Roth R, Kirchain RE (2012) Evaluating rare earth element availability: a case with revolutionary demand from clean technologies. *Environ Sci Technol* 46(6):3406–3414
- Rademaker JH, Kleijn R, Yang Y (2013) Recycling as a strategy against rare earth element criticality: a systemic evaluation of the potential yield of NdFeB magnet recycling. *Environ Sci Technol* 47(18):10129–10136
- Du X, Graedel T (2011) Global rare earth in-use stocks in NdFeB permanent magnets. *J Ind Ecol* 15(6):836–843
- Reck BK, Graedel T (2012) Challenges in metal recycling. *Science* 337(6095):690–695

6. Walton A, Han Y, Mann V, Bevan A, Speight J, Harris I, Williams A (2012) The use of hydrogen to separate and recycle NdFeB magnets from electronic waste. In: Proceedings of the 22nd international workshop on rare earth magnets and their applications, Nagasaki, Japan
7. Sheridan R, Williams A, Harris I, Walton A (2014) Improved HDDR processing route for production of anisotropic powder from sintered NdFeB type magnets. *J Radioanal Nucl Chem* 350:114–118
8. Vander HT, Blanpain B, Van Gerven T, Binnemans K (2014) From NdFeB magnets towards the rare-earth oxides: a recycling process consuming only oxalic acid. *RSC Adv* 4(109):64099–64111
9. Riaño S, Binnemans K (2015) Extraction and separation of neodymium and dysprosium from used NdFeB magnets: an application of ionic liquids in solvent extraction towards the recycling of magnets. *Green Chem* 17:2931–2942
10. Inamuddin LM, Luqman M (2012) Ion exchange technology I: theory and materials. Springer, Berlin, pp 978–994
11. Li N, Tompsett GA, Huber GW (2010) Renewable high-octane gasoline by aqueous-phase hydrodeoxygenation of C5 and C6 carbohydrates over Pt/zirconium phosphate catalysts. *ChemSuschem* 3(10):1154–1157
12. Mimura H, Lehto J, Harjula R (1997) Selective removal of cesium from simulated high-level liquid wastes by insoluble ferrocyanides. *J Nucl Sci Technol* 34(6):607–609
13. Gura V, Macy AS, Beizai M, Ezon C, Golper TA (2009) Technical breakthroughs in the wearable artificial kidney (WAK). *Clin J Am Soc Nephrol* 4(9):1441–1448
14. Alberti G, Casciola M (2001) Solid state protonic conductors, present main applications and future prospects. *Solid State Ionics* 145(1):3–16
15. Clearfield A, Stynes J (1964) The preparation of crystalline zirconium phosphate and some observations on its ion exchange behaviour. *J Inorg Nucl Chem* 26(1):117–129
16. Clearfield A, Duax W, Garces J, Medina A (1972) On the mechanism of ion exchange in crystalline zirconium phosphates-IV potassium ion exchange of α -zirconium phosphate. *J Inorg Nucl Chem* 34(1):329–337
17. Kumar CV, Chaudhari A (2000) Proteins immobilized at the galleries of layered α -zirconium phosphate: structure and activity studies. *J Am Chem Soc* 122(5):830–837
18. Casciola M, Alberti G, Donnadio A, Pica M, Marmottini F, Bottino A, Piaggio P (2005) Gels of zirconium phosphate in organic solvents and their use for the preparation of polymeric nanocomposites. *J Mater Chem* 15(39):4262–4267
19. Vivani R, Alberti G, Costantino F, Nocchetti M (2008) New advances in zirconium phosphate and phosphonate chemistry: structural archetypes. *Microporous Mesoporous Mater* 107(1):58–70
20. Sun L, Boo WJ, Sue H-J, Clearfield A (2007) Preparation of α -zirconium phosphate nanoplatelets with wide variations in aspect ratios. *New J Chem* 31(1):39–43
21. Mosby BM, Díaz A, Bakhmutov V, Clearfield A (2013) Surface functionalization of zirconium phosphate nanoplatelets for the design of polymer fillers. *ACS Appl Mater Interfaces* 6(1):585–592
22. Trobajo C, Khainakov SA, Espina A, García JR (2000) On the synthesis of α -zirconium phosphate. *Chem Mater* 12(6):1787–1790
23. Horsley S, Nowell D, Stewart D (1974) The infrared and Raman spectra of α -zirconium phosphate. *Spectrochim Acta A Mol Spectrosc* 30(2):535–541
24. Rajeh A, Szirtes L (1995) Investigations of crystalline structure of gamma-zirconium phosphate. *J Radioanal Nucl Chem* 196(2):319–322
25. Helfferich F (1995) Ion exchange. Dover, New York
26. Clearfield A (1984) Inorganic ion exchangers with layered structures. *Annu Rev Mater Sci* 14(1):205–229
27. Harvie SJ, Nancollas GH (1970) Ion exchange properties of crystalline zirconium phosphate. *J Inorg Nucl Chem* 32(12):3923–3937
28. Clearfield A, Duax W, Medina A, Smith GD, Thomas J (1969) Mechanism of ion exchange in crystalline zirconium phosphates. I. Sodium ion exchange of α -zirconium phosphate. *J Phys Chem* 73(10):3424–3430
29. Clearfield A, Troup J (1970) Mechanism of ion exchange in crystalline zirconium phosphate. II. Lithium ion exchange of α -zirconium phosphate. *J Phys Chem* 74(2):314–317
30. Lee I-H, Kuan Y-C, Chern J-M (2007) Equilibrium and kinetics of heavy metal ion exchange. *J Chin Inst Chem Eng* 38(1):71–84
31. Azizian S (2004) Kinetic models of sorption: a theoretical analysis. *J Colloid Interface Sci* 276(1):47–52
32. Alkan M, Demirbaş Ö, Doğan M (2007) Adsorption kinetics and thermodynamics of an anionic dye onto sepiolite. *Microporous Mesoporous Mater* 101(3):388–396
33. Ho Y-S, McKay G (1999) Pseudo-second order model for sorption processes. *Process Biochem* 34(5):451–465